This article was published in Separation and Purification Technology, 127, 202-211, 2014

http://dx.doi.org/10.1016/j.seppur.2014.03.007

High temperature CO_2 sorption with gallium-substituted and promoted hydrotalcites

C.V. Miguel [a], R. Trujillano [b], V. Rives [b], M.A. Vicente [b], A.F.P. Ferreira [c], A.E. Rodrigues [c], A. Mendes [a], L.M. Madeira [a,⇑]

[a] LEPABE, Department of Chemical Engineering, Faculty of Engineering, University of Porto, Rua Dr. Roberto Frias s/n, 4200-465 Porto, Portugal

[b] GIR-QUESCAT, Departamento de Química Inorgánica, Universidad de Salamanca, Plaza de la Merced, S/N, 37008 Salamanca, Spain

[c] LSRE, Department of Chemical Engineering, Faculty of Engineering, University of Porto, Rua Dr. Roberto Frias s/n, 4200-465 Porto, Portugal

Abstract

Hydrotalcites (HTC) and gallium-substituted hydrotalcites (HTC-10Ga) were prepared by co-precipitation and modified by impregnation with alkali (K and Cs) and alkaline-earth (Sr) metals. The materials were tested and screened for CO_2 sorption at 573 K. The results indicate that the modification with potassium greatly enhanced the sorption capacity when compared with the original materials (both HTC and HTC-10Ga). An outstanding sorption capacity (2.01 mmol cm^{-3} at 1.08 bar) was obtained for the sample partially substituted with gallium and modified with potassium (HTC-10Ga–20K). Moreover, this material was also submitted to sorption–desorption cycles towards CO_2 under low-pressure conditions (<0.0001–0.15 bar) to assess its use in cyclic operation. An average working capacity of 0.97 mmol cm^{-3} and 0.25 mmol cm^{-3} was obtained after repeated cycles at 573 K and 473 K, respectively. The sorption kinetics was assessed through uptake measurements, showing two parallel resistances, which were well described by the proposed model.

1. Introduction

The excessive anthropogenic greenhouse gases (GHG) emission is causing negative changes on the planet climate such as global warming, frequent events of heavy precipitation and heat waves [1]. Policies have been undertaken by developed countries in order to control, to reduce and to tax the emission of GHG like CO2. Car-bon dioxide is a relevant GHG; in fact, around 30 □ 1012 kg of CO2 per year are emitted to the atmosphere arising from the combustion of fossil fuels (coal, petroleum and natural gas) [2]. In this regard, there is a great interest in developing

technological solutions for large-scale CO2 capture, sequestration or conversion/utilization, from both the environmental and economic point of views [3].
Depending on the operating temperature, several materials (e.g. activated carbons, zeolites, metal–organic frameworks, hydrotal-cites, etc.) may be used to capture CO2 by adsorption [4,5]. Among them, hydrotalcites can be used at intermediate temperatures (473–673 K). Hydrotalcite materials are layered double hydroxides, which general formula is:

$$\left[M^{2+}_{1-x}M^{3+}_{x}(OH)_2\right][A^{n-}]_{x/n}\cdot yH_2O \qquad (1)$$

where M^{2+} and M^{3+} are divalent (e.g. Mg^{2+},Ni^{2+},Zn^{2+}, etc.) and tri-valent (e.g. Al^{3+},Ga^{3+},Mn^{3+}, etc.) metal cations, respectively. A^{n-1} is a charge balancing anion (CO^{3-},Cl^{-},SO_4^{2-}, etc.) located in the inter-layer space and x is generally between 0.2 and 0.4 [6], while y is the number of moles of hydration water located also in the inter-layer space. The mineral known as hydrotalcite has Mg^{2+},Al^{3+} and CO_3^{2-} as divalent and trivalent cations and balancing anion, respectively. Hydrotalcites can be found in nature or be synthesized. Currently, several thousands of tons of hydrotalcites are yearly produced by several chemicals companies (e.g. BASF, SASOL, Clariant, Kisuma Chemicals, Sakai Chemicals, etc.) which found application as catalysts, precursors, catalyst support, adsorbents, polymer stabilizers and antacids.
Regarding their application as an adsorbent for CO_2 capture, it has been reported that hydrotalcites exhibit a reasonably good sorption capacity, stability and easy regeneration by temperature or pressure swing [5,7–9]. Additionally, results found in the literature show that the presence of water vapour also benefits carbon dioxide sorption [10,11]. This is particularly important for CO_2 capture in applications were water vapour is present, as it is the case of coal-fired power station exhaust streams (post-combustion), or in sorption enhanced processes for H_2 production (pre-combustion) [12–14]. On the other hand, it has been reported that SOx species, also present in those streams, have a stronger affinity to hydrotalcites when compared to CO_2, despite exhibiting slower kinetics [15]; in fact, in the work by Beaver [16] it was reported that CO_2 sorption capacity on a K-promoted hydrotalcite decreased ca. 80% after exposure to CO_2/SO_2 mixtures at the end of eight successive sorption–desorption cycles.
In the work by Yavuz et al. [8], the effect of gallium substitution and modification with potassium was firstly addressed and a markedly improved CO_2 sorption capacity was observed (1.4 mmol g^1) at 473 K for a CO_2 partial pressure of 0.7 atm under dry conditions.
In this work the effect on CO_2 sorption capacity caused by gallium partial substitution and modification with potassium, cesium and strontium was evaluated and compared to that shown by the original formulation. Along with a detailed physicochemical characterization of all the prepared materials, sorption equilibrium isotherms were determined at 573 K, a typical temperature found in both post- and pre-combustion streams. Additionally, the most promising material was also submitted to sorption–desorption cycles in the low-pressure region (<0.0001–0.15 bar) at 473 K and at 573 K. Finally, the sorption kinetics was assessed for this material.

2. Experimental

2.1. Chemicals and gases

Magnesium nitrate 6-hydrate (Sigma–Aldrich, 99%), aluminium nitrate 9-hydrate (Panreac, 99.82%) and gallium nitrate hydrate (Aldrich, 99.99%) have been used as Mg, Al and Ga precursors, respectively. Anhydrous sodium carbonate (Panreac, 98.88%) was used in excess to

assure that the charge balancing anion was carbonate instead of nitrate. Sodium hydroxide (Panreac, 98.93%) was used to keep a basic pH during synthesis.
Potassium acetate (Panreac, 99%), cesium acetate (Aldrich, 99.9%) and strontium acetate (Aldrich, 99.995%) were used as chemical promoters for modifying the prepared hydrotalcite and the 10% (mol percentage) gallium-substituted hydrotalcite samples.
Carbon dioxide (99.99%) and helium (99.999%), both from L'Air Liquide, were used in the sorption experiments.

2.2. Sorbents preparation

Hydrotalcites (HTC) and hydrotalcites partially substituted with gallium (herein called HTC-10Ga) were modified by impregnation with aqueous solutions of alkaline or alkaline-earth metal cations such as K^+,Cs^+ and Sr^{2+}. The targeted not promoted hydrotalcites were $Mg_2Al(OH)_6(CO_3)_{0.5}.yH_2O$ and $Mg_2(Al_{0.9}Ga_{0.1})(OH)_6(CO_3)_{0.5}.yH_2O$. The two previously mentioned samples, respectively HTC and HTC-10Ga, were prepared by the co-precipitation method. In the work by Yong et al. [9] the CO_2 sorption capacity was determined at 573 K for three commercial hydrotalcites from SASOL having different Mg/Al ratios: 0.4, 1.0 and 2.3. It was observed that an Mg/Al ratio of 1 had the highest sorption capacity followed by 2.3 and, finally, by 0.4. However, the lowest limit of the Mg/Al ratio for obtaining crystallographically pure hydrotalcite (2.0) is attributed to electrostatic repulsion between neighbouring, octahedrally coordinated, trivalent metals in the layers, which is unavoidable if Mg/Al is lower than 2 [6]. For this reason, and based on the results obtained by Yong et al. [9], molar ratios of 2 were chosen for Mg^{2+}/Al^{3+} and $Mg^{2+}/(Al^{3+}+Ga^{3+})$, while for the Ga-containing sample an Al:Ga ratio of 9:1 was also considered (see method details in [6]) to check the effect of gallium presence.
The solution containing the divalent and trivalent cations was drop-wise added to the basic solution containing NaOH and Na_2CO_3. The resulting solution was continuously stirred during 17 h at room temperature and then the suspension was centrifuged and the solids washed with distilled water for removing nitrate an-ions and sodium cations. The samples were then dried at 308–323 K and crushed. Both samples (HTC and HTC-10Ga) were then calcined at 673 K during 2 h in air and the loss of mass assessed in order to further prepare the alkali modified samples with a pre-established stoichiometry. So, part of the remaining HTC sample was modified with K while three parts of the HTC-10Ga sample were modified with K, Cs or Sr (cf. Table 1) by impregnation to accomplish a 20 wt.% loading. This content is typically found in other works [7,14,17] following the important work by Hufton et al. [18], although it has been reported that the sorption capacity at 673 K is not appreciably changed when using different loadings [13,18]. Impregnation was followed by drying (313–323 K), crushing, and calcination at 673 K during 2 h in air.

Table 1. List of prepared samples

Sample	M^{2+}	M^{3+}		A^{n-}	Promoter (wt.%)	
HTC	Mg	Al	–	CO_3	–	–
HTC-20K	Mg	Al	–	CO_3	K	20%
HTC-10Ga	Mg	Al	Ga	CO_3	–	–
HTC-10Ga–20K	Mg	Al	Ga	CO_3	K	20%
HTC-10Ga–20Cs	Mg	Al	Ga	CO_3	Cs	20%
HTC-10Ga–20Sr	Mg	Al	Ga	CO_3	Sr	20%

2.3. Sorbents characterization

The HTC and HTC-10Ga materials were analysed by thermo-gravimetric analysis (TG/DTG) in a TA Instruments apparatus, Model SDT Q600, to study their thermal stability. Each sample was heated at 10 K min^{-1} up to 1273 K in a dynamic air atmosphere.

Powder X-ray diffraction (PXRD) patterns were recorded in a Siemens D500 diffractometer equipped with DIFFRACT-AT software, using Cu Kα radiation (k = 1.5405 Å), a Ni filter and a graphite monochromator. The analysis conditions were: 40 kV, 30 mA, a step size of 0.05° and a scanning speed of 2° (2 theta) per minute.

Fourier Transformed Infrared Spectroscopy (FTIR) (Perkin–Elmer, 1600 Series) was performed in the range 4000–400 cm^{-1} using the KBr technique. Scanning Electron Microscopy (SEM) was performed on a JEOL JSM 6301F instrument coupled with Energy Dispersive Spectroscopy (EDS) (JEOL JSM 6301F/Oxford INCA Energy 350) to investigate the materials structure and composition. The textural properties of the prepared materials were obtained by means of nitrogen adsorption at 77 K (Micrometrics, model Gemini II), after degassing the samples for 2 h at 383 K in a Flowprep 060 apparatus (Micrometrics).

High temperature CO_2 sorption measurements were performed using a magnetic suspension balance from Rubotherm. First, the sample (ca. 1 g) was heated overnight up to 585 K under vacuum (<0.001 bar) followed by a buoyancy determination with He at 313 K, which allowed to determine the solid density after the regeneration step. Equations for buoyancy correction can be found in the Supplementary Information Section. Subsequently, the sample was again heated up to the desired temperature and CO_2 fed to the chamber until reaching the required pressure for measuring the first sorption equilibrium value. The uptake curve was recorded by an automated data acquisition system. The equilibrium was considered to be reached when a variation of less than 0.1 mg was observed during 20 min. For screening purposes the sorption equilibrium values were obtained at 573 K and for CO_2 pressures of ca. 0.05, 0.15, 0.45 and 1.10 bar. Afterwards, the most promising material was submitted to sorption–desorption cycles at 573 K and 473 K and the reversible/steady working capacity determined. Typically, the carbon dioxide partial pressure in post-combustion flue gases is 0.15 bar and so each cycle consisted in increasing the pressure up to 0.15 bar followed by desorption down to vacuum, except for cycle number 3 where the pressure was increased up to 1.1 bar to check the effect of the feed pressure on the cyclic stability.

3. Results and discussion

3.1. Sorbents physicochemical characterization

3.1.1. TG/DTG

Thermogravimetric analysis was performed to study the thermal decomposition of HTC and HTC-10Ga fresh samples (Fig. 1); a total mass loss of 55% and 47% was found, respectively. Both

samples show three DTG peaks related to the removal of hydration water and hydroxyl groups (at 353–373 K and 463 K) and carbon-ate anions (at 653 K), as discussed in detail elsewhere [19,20].As mentioned in Section 2.2, the fresh samples were calcined at 673 K for further studies, as this treatment ensures that all water existing in the fresh samples is removed. The used calcination temperature is in line with several works [7,8,21] and was also chosen following the study by Ram Reddy et al. [22], where it was observed that samples calcined at 673 K provided a higher CO_2 sorption capacity. Moreover, this is the highest operation temperature expected to be used in most final applications (e.g. for pre-combustion CO_2 capture).

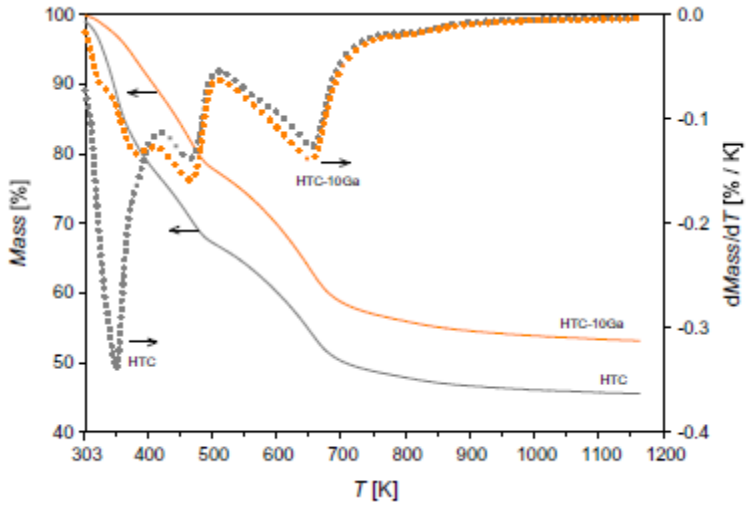

Fig. 1. Thermogravimetric (TG) (solid lines) and derivative thermogravimetry (DTG) (dotted lines) analysis of the fresh samples HTC and HTC-10Ga.

3.1.2. XRD

The XRD patterns of the samples calcined at 673 K corresponded to mostly amorphous materials, where only weak and broad signals due to MgO were observed; the pattern for the Ga-containing sample is shown in Supplementary Information (Fig. S.1). This result is in agreement with the TG curve (Fig. 1), which showed that at 673 K most of the removable mass has been eliminated (water vapour and carbonates), leaving the mostly amorphous solid. However, the XRD patterns evidenced that one year after their synthesis, calcination at 673 K and storage, all the materials have a typical hydrotalcite structure, suggesting that upon exposure to humid air the materials have reconstructed their layered structure [23] (Fig. 2a).

The partial substitution with gallium led to an increased height intensity of the d(0 0 3) peak (see patterns of samples HTC and HTC-10Ga in Fig. 2a). Impregnation with cesium (HTC-10Ga–20Cs) did not result in large enough crystals that could be identified by XRD, meaning that cesium is well dispersed on the material. For the case of impregnation with strontium, a strontianite crystal-line phase ($SrCO_3$) was identified (JCPDS file 5-0418), while $K_2CO_3.1.5\ H_2O$ (JCPDS file 11-0655) was verified in both samples impregnated with potassium.

After CO_2 sorption the XRD patterns showed important differences. Representative diagrams are included in Fig. 2b. First of all, the maxima due to the layered hydrotalcite structure (easily observed in the sample stored for one year) have vanished completely for sample HTC-10Ga–20Sr or decreased markedly their intensities for other samples (although the bands due to $SrCO_3$ remained unaltered). This behaviour is due to two complementary facts: (i) the CO_2 capture experiments were carried out at 573 K (after outgassing the sample at 585 K), a temperature

high enough to destroy the layered structure, as concluded from the TG results above mentioned (Fig. 1); (ii) despite the presence of a high pressure of CO_2 would hopefully give rise to recovering the layered structure (the so-called ''memory effect'') [24,25], it should be stressed that the experiments were carried out in the absence of water vapour, and thus the hydrotalcite-like structure could not be recovered. When the sample was submitted to five consecutive CO2 sorption–desorption cycles the XRD patterns did not show any significant difference (cf. Fig. 2b), although some minor sharpening of the maxima was observed when the cycles were carried out at 573 K, but not at 473 K. Probably, this treatment at the higher temperature in some sort of way favoured an incipient crystallization of the existing crystalline phases.

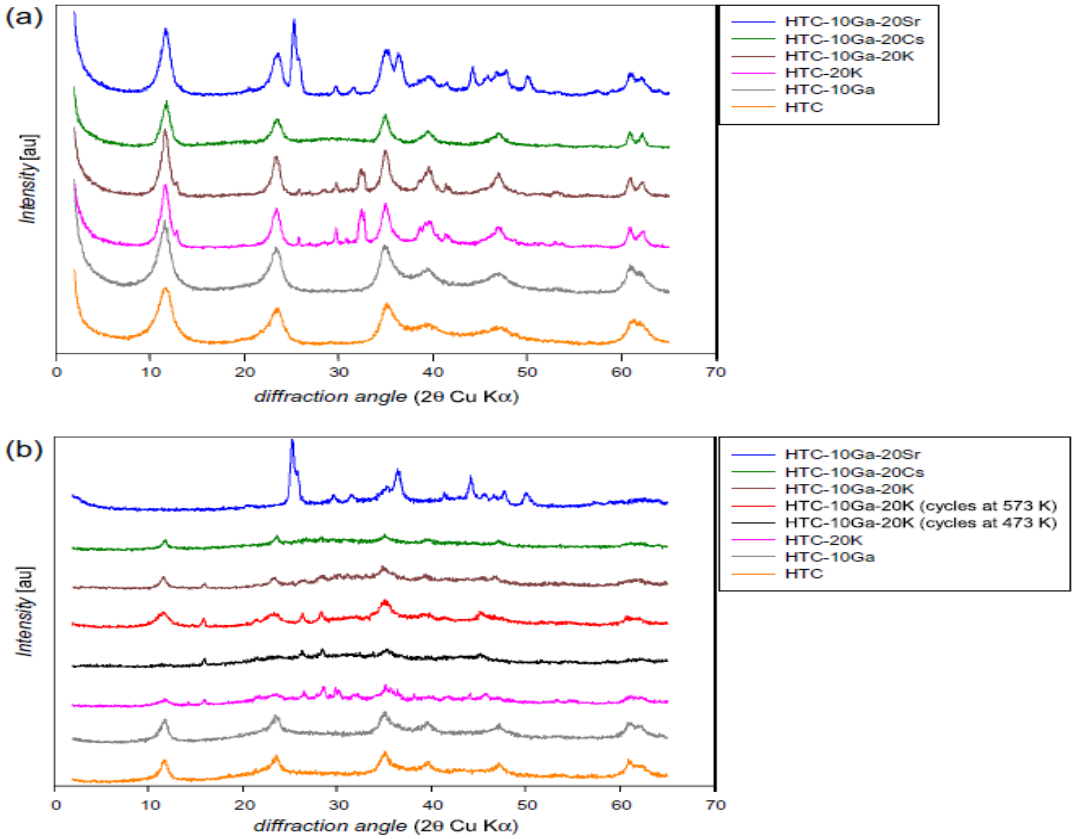

Fig. 2. XRD patterns of samples: (a) one year after being calcined at 673 K and stored, and (b) after CO_2 sorption.

3.1.3. SEM/EDS

SEM images evidenced that the samples exhibit a not defined and/or regular shape (Fig. 3), excepting HTC-10Ga–20Sr (pattern e) and, particularly, HTC-20K and HTC-10Ga–20K (patterns c and f), which also revealed the presence of zones of the needle-like (Z1) or flat surface (Z3) type. This was already observed by Oliveira et al. [7] using commercial hydrotalcites modified with potassium. Interestingly, EDS analysis allowed to verify that the potassium mass content at the flat surface zones is the same for both HTC-20K and HTC-10Ga–20K samples (26 wt.%). This content is also much higher than on the bulk material (7 wt.%) and needle-like zones (5 wt.% vs. 14 wt.%, respectively) (see Fig. S.2 in Supplementary Information). Although incipient wetness impregnation usually leads to a homogeneous distribution of the active phase, it is clear that K has a marked preference to deposit in certain zones of the supports.

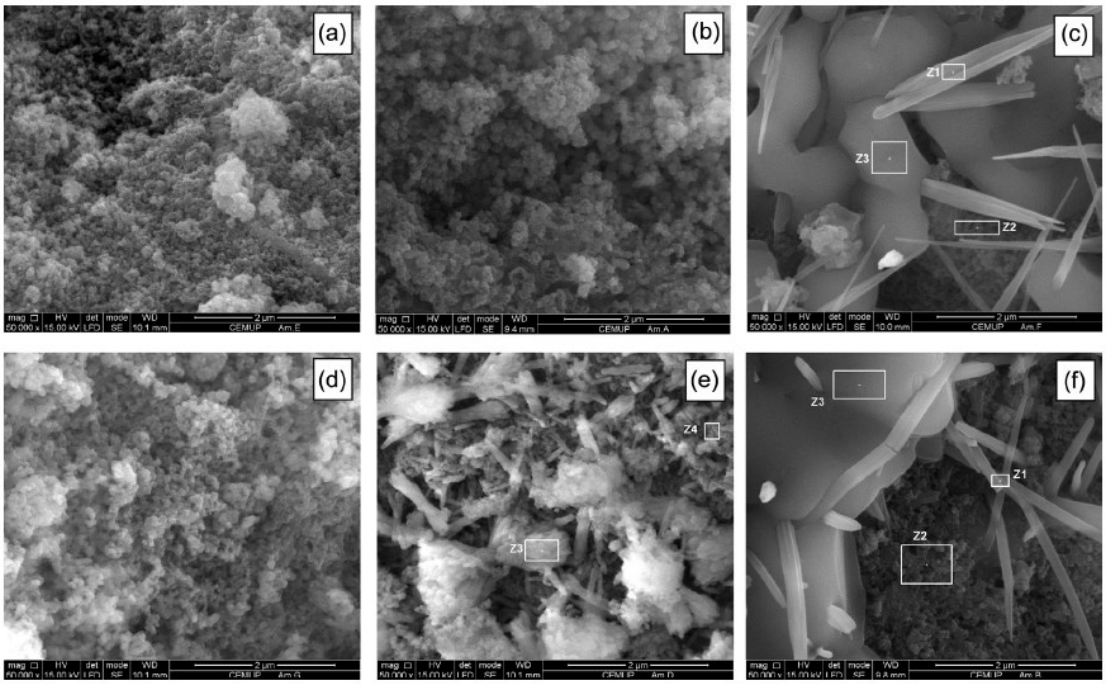

Fig. 3. SEM images of the prepared materials: (a) HTC, (b) HTC-10Ga, (c) HTC-20K, (d) HTC-10Ga–20Cs, (e) HTC-10Ga–20Sr and (f) HTC-10Ga–20K.

3.1.4. Physical adsorption of nitrogen at 77 K

The specific surface areas were determined by physical adsorption of N_2 at 77 K (cf. Table 2). Type II isotherms were obtained (see Supplementary Information – Fig. S.3), which means that the resulting materials are macroporous/mesoporous solids; the deter-mined volume of microporous (<0.005 cm^3 g^{-1}) can be neglected. The specific surface area increased after calcination, particularly in the case of the HTC sample (ca. 50% of increase). This is related to dehydration followed by collapse of the layered structure that occurs upon calcination at 673 K [26]. Nevertheless, the modification with alkali metals (K and Cs) resulted in lower specific surface areas, being this fact more evident when the hydrotalcites were modified with potassium. In fact, both samples modified with potassium (HTC-20K and HTC-10Ga–20K) have nearly the same specific surface areas, being the lowest observed. Probably this is related to pore blocking caused by the K_2CO_3 phase, which is in agreement with SEM images (cf. Fig. 3c and f). The modification with an alkaline earth metal (Sr) resulted in the material with the highest specific surface area (SBET = 237 m^2 g^{-1}). Although a straightforward explanation is lacking for this behaviour, it might be tentatively related to subtle changes in the basicity of the media upon addition of the doping cations.

Table 2. BET specific surface area of the prepared materials determined by physical adsorption of nitrogen at 77 k

Sample	S_{BET} ($m^2\ g^{-1}$)
HTC (fresh)	122
HTC (calcined)	183
HTC-20K (calcined)	61
HTC-10Ga (fresh)	156
HTC-10Ga (calcined)	175
HTC-10Ga–20K (calcined)	58
HTC-10Ga–20Cs (calcined)	165
HTC-10Ga–20Sr (calcined)	237

3.1.5. FTIR

FTIR analyses obtained for the as prepared (uncalcined) HTC and HTC-10Ga samples indicate the presence of carbonate as inter-layer anion (cf. Fig. 4). The spectra show an intense, broad band centered at ca. 3460 cm□1, due to the stretching mode of the hydroxyl groups, both from the brucite-like layers and the interlayer water molecules, as well as the water molecules physisorbed on the external surface of the crystallites. The shoulder at 2900–3000 cm^{-1} has been ascribed [27] to the stretching mode of inter-layer hydroxyl groups hydrogen-bonded to interlayer carbonate species. The bending mode of the water molecules is responsible for the rather weak band at ca. 1630 cm^{-1}, also recorded for both samples. The υ3 mode of interlayer carbonate is responsible for the intense band at 1384 cm^{-1}. This is a degenerated mode for the D_{3h} symmetry of the original carbonate anion; under this symmetry, the υ1 mode expected at ca. 1080 cm^{-1} is inactive and it is not recorded. However, it can be noticed that the band at 1384 cm^{-1} shows a clearly identified shoulder at 1500 cm^{-1}, which can be considered as a result of the splitting of the υ3 mode. However, as the band due to the m1 mode is not recorded, the decrease in the symmetry should be discarded and the two bands at 1384 and 1500 cm^{-1} should be ascribed to carbonate species in two sites with different interaction with their local environment. Weaker bands below 1000 cm^{-1} correspond mainly to vibration of lattice bonds (Mg–OH, Al–OH, etc.).

When the samples were calcined at 673 K the spectra showed some differences, but unfortunately it seems that some interlayer carbonate species are still present (it should be noticed that at this temperature not all carbonate has been removed, cf. the TG curve –Fig. 1); the hydroxyl groups have not been completely removed either. Consequently, the spectra show the band at ca. 3450 cm^{-1} due to the stretching mode of the hydroxyl groups (although the band is much narrower than for the uncalcined samples), and the hydrogen bonding between the hydroxyl groups and the carbonate species seem to be absent. The remaining carbonate species show a lower symmetry and the υ3 mode has lost its original degeneration, probably on changing the carbonate anion from a D_{3h} to a $C_{2υ}$ symmetry, the corresponding band is now split into two bands at ca. 1480 and 1410 cm^{-1} and the band due to mode υ1 is now recorded at 1110 cm^{-1}.

Impregnation with Sr, K, or Cs and calcination at 673 K leads to some changes in the spectra, concerning almost exclusively to the region below 1600 cm^{-1}. The band due to mode υ3 of carbonate species splits in all cases and the band due to mode υ1 of carbonate is recorded in all cases as well, indicating that in this case a decrease in the local symmetry of the carbonate anions actually has taken place. However, both components of the split υ3 band show a change in their relative intensities from the monovalent (K and Cs) to the divalent (Sr) doping cation; this might be tentatively related to the different nature (mono- or divalent) of the doping cations. Probably, the increased basicity of the solids after impregnation with the alkaline or

alkaline-earth cations delays decomposition of the solid and evolution of CO_2, and thus remaining of carbonate species above the temperature where decomposition, in the absence of the doping cations, would be expected. Moreover, if carbonate species still exist after calcination at 673 K, this would account for the shoulder around 2900 cm^{-1} due to the υOH stretching mode of hydroxyl groups hydrogen-bonded to the carbonate species.

The absence of bands around 1700–1750 cm^{-1} indicates that although acetate salts were used for modifying the hydrotalcites with K, Cs and Sr, no ion exchange between acetate and interlayer carbonate ions, within the hydrotalcite structure, took place.

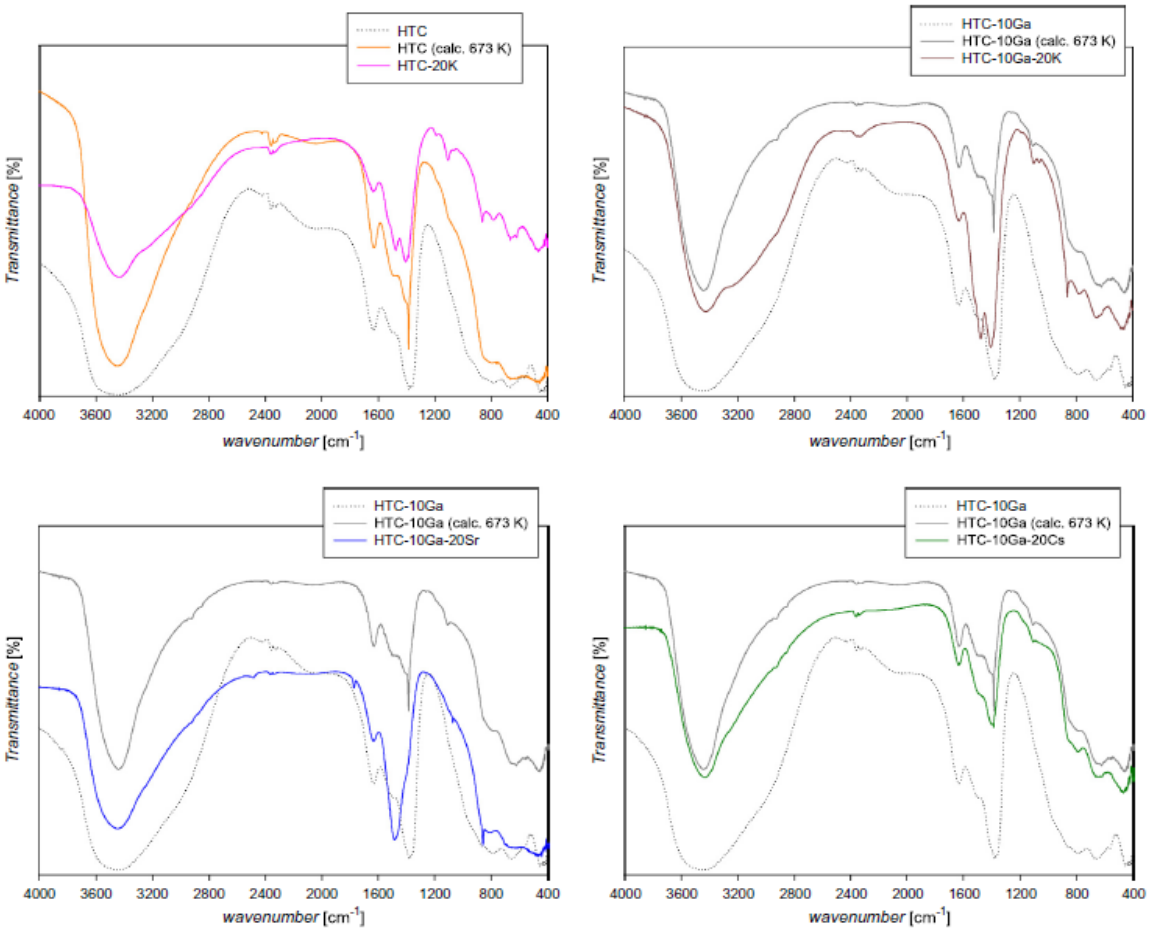

Fig. 4. FTIR spectra of the starting and modified samples

3.2. CO2 sorption experiments

3.2.1. Determination of sorption equilibrium isotherms at 573 K –sorbent screening

Fig. 5 shows CO_2 sorption isotherms obtained at 573 K under dry conditions for the prepared materials. The results are very promising, particularly for the sample substituted with gallium and modified with potassium (HTC-10Ga–20K); a sorption equilibrium value of 1.82 mmol g^{-1} (i.e., 2.01 mmol cm^{-3}) at 1.08 bar was obtained which is, up to the authors knowledge, clearly above typical results found in the literature under similar operation conditions (see Table 3) [9,22,28,29].

Generally, the modification with alkali metals increases the sorption capacity of the original hydrotalcite samples (HTC and HTC-10Ga). However, adding potassium provided higher sorption values when compared to cesium and this should be related to its higher basicity. On the contrary, the sorption capacity decreased for the sample modified with an alkaline-earth metal (Sr). More-over, the sorption capacity of the materials decreased in general with the increase of

their specific BET surface area (cf. Table 2 and Fig. 5). This means that the available BET surface area does not play a crucial role on the sorption capacity, which was also re-ported in other works [7,30]; the sorption capacity is more likely to be related to the chemical nature of the exposed surface. In the case of HTC-10Ga–20Sr it seems that the phase obtained (strontianite), which has a completely different morphology (see Fig. 3e), almost does not sorb CO_2, at least under the tested operation conditions.

The results herein presented are in line with the ones obtained by Yavuz et al. [8], where they showed that the simultaneous modification with potassium and gallium markedly improved the sorption capacity of hydrotalcites, the first acting as a chemical promoter and the latter providing a superstructure robust and stable at elevated temperatures (a sort of synergic effect). However, in our work the sorption isotherm was obtained at 573 K and up to 1.1 bar. Moreover, this promising sample (HTC-10Ga–20K) was also submitted to sorption–desorption cycles at 573 K and 473 K to determine its reversible working capacity, checking its suitability to be used in cyclic operation for post-combustion CO_2 capture/valorisation applications (Section 3.2.2).

The sorption data of each sample was fitted to the Freundlich equation (Eq. (2)), which has also been proposed elsewhere to de-scribe CO_2 sorption on hydrotalcites [21,31]:

$$q = Kp^{\frac{1}{n}} \qquad (2)$$

where q (mmol cm^{-3}) is the concentration of the sorbed species, and K (mmol cm^{-3} $bar^{-(1/n)}$) and n (dimensionless) are Freundlich equation parameters. Parameter n is normally greater than unity and as it increases the isotherm approaches to the so-called irreversible isotherm. In this case, the pressure needs to be very low in order to the sorbate start desorbing from the surface [32].

The parameters of the Freundlich equation (along with a 90%interval of confidence) are included in Table 4. The experimental data of the starting and modified samples showed good adhesion to the Freundlich model within the tested pressure range (see also Fig. 5).

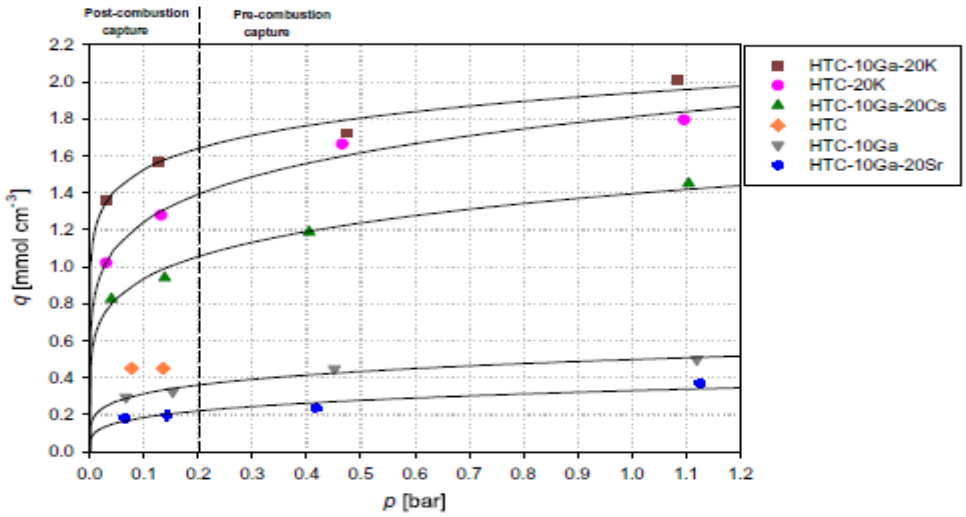

Fig. 5. CO_2 sorption equilibrium isotherms at 573 K for the prepared materials. Lines shows fitting using the Freundlich equation

3.2.2. Sorption–desorption experiments

In order to determine the working capacity of the best sorbent (HTC-10Ga–20K), a series of sorption–desorption cycles at 573 K and 473 K was carried out. As it can be seen in Fig. 6, in what we called cycle 0, CO_2 was fed to the microbalance chamber and the pressure allowed to increase up to 0.05 bar and then to 0.15 bar. Each cycle ended with the sample being submitted to vacuum. In this cycle, the sorption capacity determined at 573 K and 0.15 bar (Fig. 6a) was 1.57 mmol cm^{-3}. However, when the micro-balance chamber was evacuated it was not possible to remove all the sorbed CO2; around 0.38 mmol cm^{-3} remained sorbed – see open symbol. In the following cycles the pressure was again switched between 0.15 bar and vacuum, except in cycle 3 where the pressure was increased up to 1.1 bar before the regeneration stage. It is important to note that the sorption values presented in each cycle (black symbols) correspond to the working capacity, i.e., it was considered a starting mass of the sample which included the previous irreversibly sorbed mass of CO2. For instance, in cycle 1 at 573 K, the sample was able to effectively sorb only 1.13 mmol cm^{-3}, which is smaller than the value in cycle 0 because some carbon dioxide remained irreversibly sorbed. By adopting this approach it is thus possible to determine the working capacity in each cycle. Fig. 6 shows that just after cycle 2 a steady working capacity is mostly attained; at 573 K this working capacity is ca. 0.97 mmol cm^{-3} whereas at 473 K it is ca. 0.25 mmol cm^{-3}. However, at the end of the first cycle, around 24% and 77% of the total sorption capacity is irreversibly lost at 573 K and 473 K, respectively (cf. Figs. 7 and 8). In Fig. 7 the irreversible fraction at the end of each cycle is determined as the difference between the black and white bars (for instance in cycle 0 at 573 K such value is the one mentioned above, 0.38 mmol cm^{-3}). The irreversible part was found to be also pressure dependent as shown in Fig. 8, where the accumulated irreversible fraction is shown; it is noteworthy that when the pressure was increased up to 1.1 bar (i.e. during cycle 3), the number of moles of CO_2 that were irreversible sorbed increased 51% and 72% at 573 K and 473 K, respectively. However, in the subsequent cycles the working capacity remained nearly constant at each temperature.

The obtained results suggest that the CO_2 sorption takes place through an activated process; otherwise, it would be expected to obtain a higher sorption capacity at 473 K. In this regard, several authors proposed different models to describe the sorption equilibrium of carbon dioxide over hydrotalcites [7,28,33], although in the present work a good fit was obtained using a simple Freundlich equation (Section 3.2.1).

The changes observed in the CO_2 sorption capacity during the implemented cyclic process in the absence of water vapour can be, in principle, related to the structural changes observed by XRD, in which the hydrotalcite-like structure could not be recovered. Further work should thus aim assessing the behaviour of these materials in the presence of water vapour, which is found in both typical post- and pre-combustion streams. In fact, other authors found that in presence of water the working capacity loss practically does not occur (<10%) as compared to that exhibited by the same material under dry conditions [12].

Regarding the sorption mechanism, Ritter and co-workers [34] observed, from in situ FTIR spectroscopy, the carbonate transformations occurring in K-promoted hydrotalcites during CO_2 adsorption and desorption at 723 K. In their study, it was observed that one irreversible and three reversible processes took place simultaneously, that could somehow be represented by two distinct kinetic contributions. The slow and irreversible process was related to the formation of polydentate carbonate, whereas the fast and reversible uptakes were related to the formation of bridged (sur-face), uni- and bidentate carbonate species. Ritter and co-workers concluded that the formation of bidentate carbonate species is favoured at very short times. Unidentate and bridged carbonate species start to disappear after one hour, eventually due to their transformation into polydentate carbonate. In order to preliminary assess the sorption kinetics of sample HTC-10Ga–20K, based on the above mentioned findings, the following

expression is herein pro-posed to tentatively describe the total amount of substance entering or leaving the sorbent particle [35]:

$$F = \frac{q(t) - q(t=0)}{q(\infty) - q(t=0)} = \left(1 - \frac{6}{\pi^2}\sum_{i=1}^{\infty}\frac{1}{i^2}e^{\left(-i^2\pi^2\frac{D_1}{r^2}t\right)}\right)\frac{q_1}{q_\infty} + \left(1 - \frac{6}{\pi^2}\sum_{i=1}^{\infty}\frac{1}{i^2}e^{\left(-i^2\pi^2\frac{D_2}{r^2}t\right)}\right)\frac{q_2}{q_\infty} \quad (3)$$

Eq. (3) assumes constant surface concentration in the sorbent particle and two kinetic contributions occurring in parallel, one responsible for the fast uptake at the beginning and, the other one, by the slow increase observed for longer times. The model parameters $\frac{D1}{r^2}(s^{-1})$, $\frac{D2}{r^2}(s^{-1})$ and q1 (mmol cm^{-3}) were obtained through non-linear fitting of Eq. (3) to experimental data. One should note that q1 (mmol cm^{-3}) is known, since it is equal to the difference between the sorbed (or desorbed) quantity at equilibrium and the value for t = 0. Additionally, the quantity related to the slow uptake, q2 (mmol cm^{-3}), is equal to the difference between q1 (known a priori) and q1 (fitted parameter).

Fig. 9 shows the experimental uptake (F), downtake (1-F) and model curves based on Eq. (3), where F is the sum of curves F1 and F2 (please see Fig. S.4 in the Supplementary Information for the total and partial loading uptake curves). The model predicts quite well the experimental data both during sorption and desorption at 573 K and 473 K; the obtained parameters are shown in Table 5. Generally, the inverse of the time constant $\frac{D1}{r^2}$ is twofold higher than $\frac{D2}{r^2}$

When compared the uptakes performed at the beginning of the experiment on the reactivated sample (cycle 0) and at the end (cycle 5), it is observed that the inverse of time constants $\frac{D1}{r^2}$ and $\frac{D2}{r^2}$ decreased for both temperatures, being this growth more noticeable at 473 K. Regarding $\frac{D2}{r^2}$

A small decrease with cycling was observed at both temperatures.

The sorbed fraction related to the first contribution q1/q∞ increased between cycles (13 percentage points) at 473 K, while at 573 K practically remained constant. Desorption is much faster at 473 K where ca. 63% of the total desorbed quantity is related to the fast contribution whereas at 573 K represents only 11%.

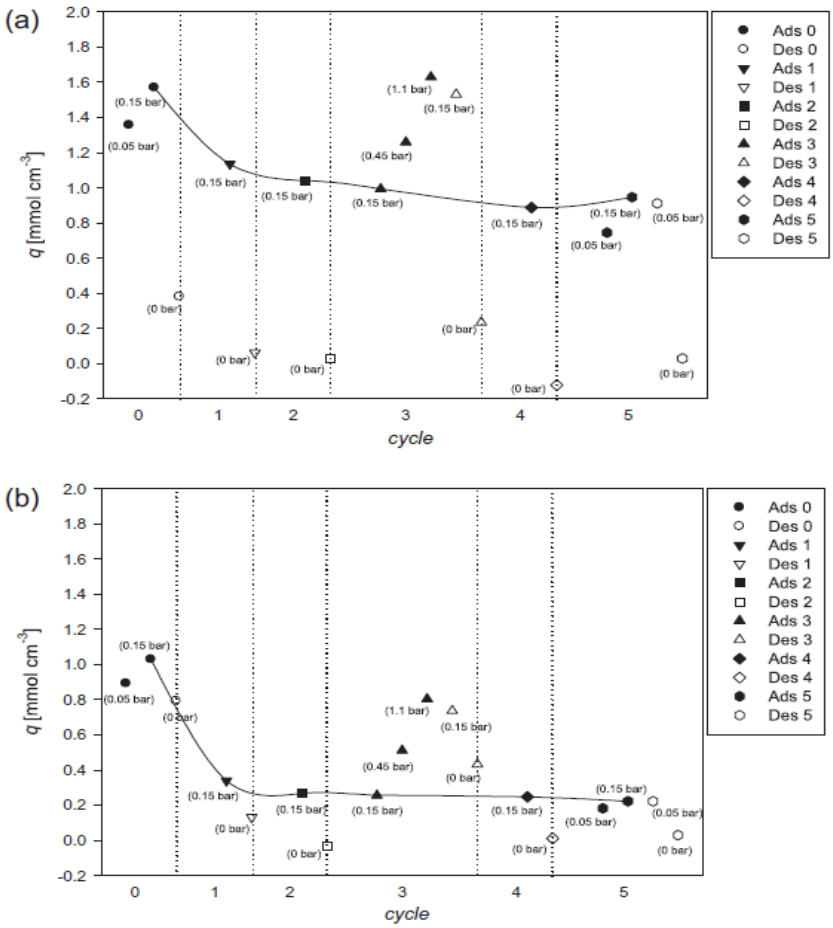

Fig. 6. Working capacity of HTC-10Ga–20K towards CO2 (see guiding solid line) obtained after consecutive sorption–desorption cycles at: (a) 573 and (b) 473 K.

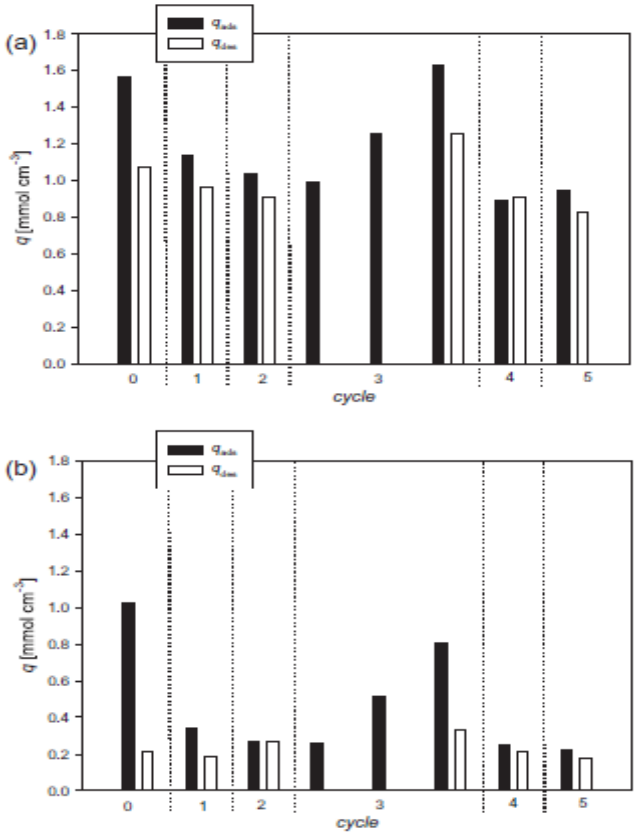

Fig 7. History of sorbed (black bars) and desorbed (white bars) amount of CO2 for each cycle at (a) 573 K and (b) 473 K.

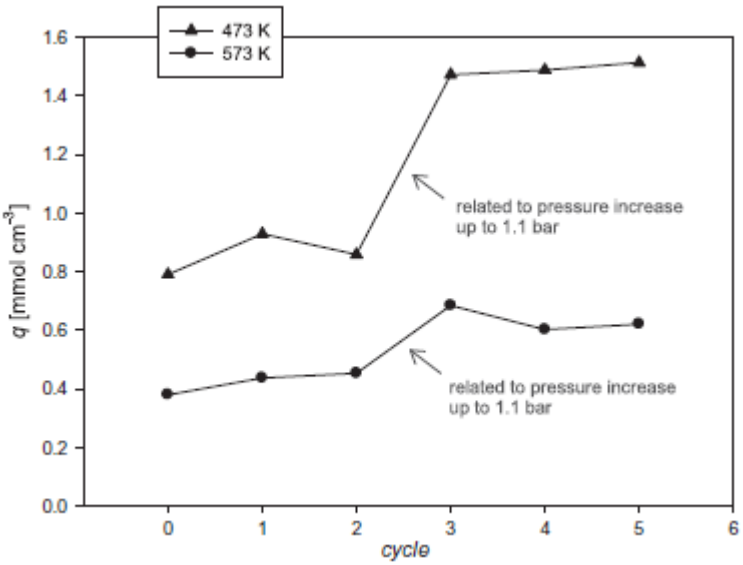

Fig. 8. Irreversible CO_2 moles sorbed per cycle considering the mass of solid obtained after the first regeneration step at 473 K and 573 K. Lines are for eye guidance.

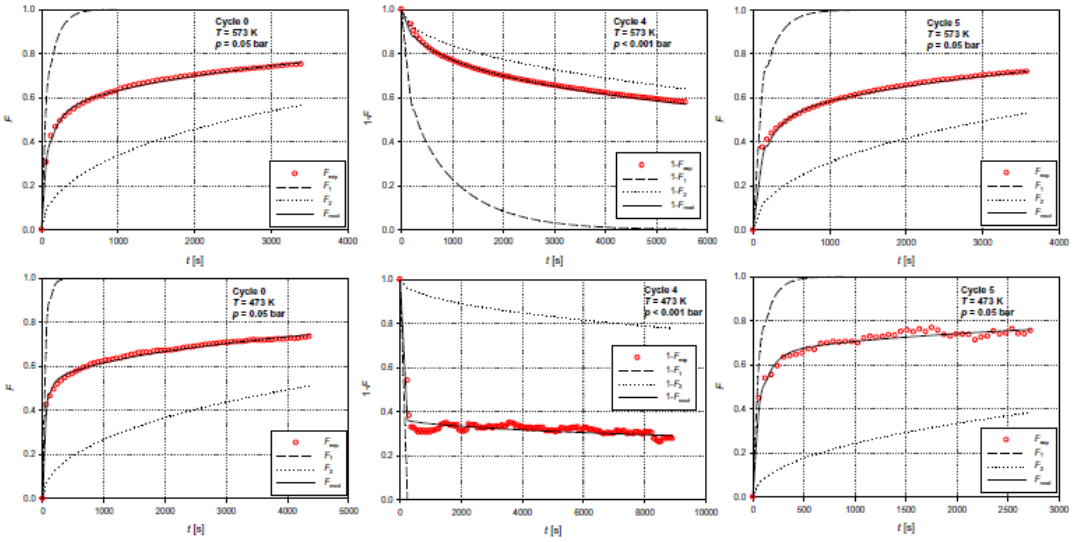

Fig. 9. Uptake (and downtake) curves for CO_2 sorption at 573 K (first row) and 473 K (second row) for sample HTC-10Ga–20K.

Table 3. Carbon dioxide sorption equilibrium value on HTC-10Ga-20K and comparison with other sorbents reported in the literature.

Material	T (K)	p_{CO2} (bar)	q (mol kg^{-1})	Ref.
HTC-10Ga–20K	573	1.08	1.82	This work
Hydrotalcite	573	1	0.52	[29]
Hydrotalcite	573	1	0.50	[9]
Hydrotalcite	573	1.1	0.25	[22]
K-promoted hydrotalcite	673	1	0.79	[28]

Table 4. Freundlich type isotherm parameters and their confidence limits (90%) obtained after fitting the experimental data of Fig. 5 (T = 573 K) and solid density (determined with He at 313 K after regeneration) for each material.

Sample	log (K)	$1/n$	R^2	ρ (g cm^{-3})
HTC	–	–	–	0.831
HTC-20K	0.26 ± 0.034	0.16 ± 0.038	0.9875	0.841
HTC-10Ga	−0.30 ± 0.055	0.20 ± 0.074	0.9685	0.860
HTC-10Ga–20K	0.29 ± 0.035	0.10 ± 0.039	0.9685	1.107
HTC-10Ga–20Cs	0.14 ± 0.046	0.17 ± 0.054	0.9774	1.187
HTC-10Ga–20Sr	−0.48 ± 0.11	0.25 ± 0.15	0.9251	0.762

Table 5. Kinetic parameters of Eq. (3) obtained after fitting CO_2 uptakes and downtakes at 573 K and 473 K on sample HTC-10Ga–20K.

Parameter	Cycle 0 p = 0.05 bar (uptake)		Cycle 4 p < 0.001 bar (downtake)		Cycle 5 p = 0.05 bar (uptake)	
	473 K	573 K	473 K	573 K	473 K	573 K
$\frac{D_1}{r^2} \times 10^4$ (s^{-1})	15.55	7.57	117	1.00	9.08	4.88
$\frac{D_2}{r^2} \times 10^6$ (s^{-1})	7.41	12.26	0.55	2.54	6.01	9.91
$\frac{q_1}{q_{sat}} \times 100$	48	44	63	11	61	40

4. Conclusions

Hydrotalcite-based materials were prepared and their sorption capacity towards CO_2 at high temperature was determined. The working capacities obtained under low CO_2 pressures and high temperatures are lower than those typically observed in absorption units using amines operating at low temperatures (i.e. 1.36 mmol g^{-1}), which however require that the flue gas stream should be cooled (and later on heated up to for the solvent regeneration stage). Nevertheless, at 573 K the hydrotalcites capacities are clearly above the minimum value (i.e. 0.3 mmol g^{-1}) considered for their application in pre-combustion capture applications, particularly in sorption-enhanced reaction processes. The sorption capacity was enhanced by partially substituting aluminium with gallium and, particularly, after modifying with alkali metals (K and Cs). The sorption equilibrium isotherms for all the materials were adequately fitted using a simple Freundlich-type equation.

The best material, i.e. hydrotalcite substituted with gallium and promoted with potassium (HTC-10Ga–20K), showed to be suitable to be used in cyclic operation with regeneration under low CO_2 pressure, particularly at 573 K, where a very good working capacity (0.97 mmol cm^{-3}) was obtained. At 473 K, more than 75% of the sorption capacity was irreversibly lost and a low working capacity is thus obtained (0.25 mmol cm^{-3}). However, as mentioned before, it is known that in presence of water vapour such working capacity should be almost not affected.

Sorption kinetics of the HTC-10Ga–20K material was preliminary assessed and a model proposed considering two resistances in parallel. The model showed good adherence to experimental data both during sorption and desorption experiments; the inverse of the time constant related to the fast uptake is generally twofold higher than the slow uptake.

Acknowledgments

This work is supported by project PTDC/EQU/ERQ/098730/2008, financed by the European Fund for Regional Development (ERDF) through COMPETE – Programa Operacional Factores de Competitividade – and by Fundação para a Ciência e a Tecnologia (FCT).

C.V. Miguel is grateful for his research grant under the project NORTE-07-0124-FEDER-000026, financed by ERDF through Programa Operacional do Norte (ON2) and by national funds from FCT/MEC (PIDDAC).

The authors also acknowledge financial support through a Portugal-Spain Cooperation Project (PT2009-0057 and Integrated Action No E-59/10). Funds from the Spanish Ministry for Science and Innovation (MAT 2009-08526) and ERDF are also acknowledged.

References

[1] IPCC: Summary for Policymakers, in: T.F. Stocker, D. Qin, G.-K. Plattner, M. Tignor, S.K. Allen, J. Boschung, A. Nauels, Y. Xia, V. Bex, P.M. Midgley (Eds.), Climate Change 2013: The Physical Science Basis. Contribution of Working Group I to the Fifth Assessment Report of the Intergovernmental Panel on Climate Change, Cambridge University Press, Cambridge, United Kingdom and New York, NY, USA, 2013.

[2] J. Wilcox, Carbon Capture, Springer, New York, 2012.

[3] E.A. Quadrelli, G. Centi, J.L. Duplan, S. Perathoner, Carbon dioxide recycling: emerging large-scale technologies with industrial potential, ChemSusChem 4 (2011) 1194–1215.

[4] S. Choi, J.H. Drese, C.W. Jones, Adsorbent materials for carbon dioxide capture from large anthropogenic point sources, ChemSusChem 2 (2009) 796–854.

[5] Q. Wang, J. Luo, Z. Zhong, A. Borgna, CO2 capture by solid adsorbents and their applications: current status and new trends, Energy Environ. Sci. 4 (2011) 42–55.

[6] A. de Roy, C. Forano, J.P. Besse, Layered double hydroxides: synthesis and post-synthesis modification, in: V. Rives (Ed.), Layered Double Hydroxides: Present and Future, Nova Science Publishers Inc., New York, 2001, pp. 1–39.

[7] E.L.G. Oliveira, C.A. Grande, A.E. Rodrigues, CO2 sorption on hydrotalcite and alkali-modified (K and Cs) hydrotalcites at high temperatures, Sep. Purif. Technol. 62 (2008) 137–147.

[8] C.T. Yavuz, B.D. Shinall, A.V. Iretskii, M.G. White, T. Golden, M. Atilhan, P.C. Ford, G.D. Stucky, Markedly improved CO2 capture efficiency and stability of gallium substituted hydrotalcites at elevated temperatures, Chem. Mater. 21 (2009) 3473–3475.

[9] Z. Yong, V. Mata, A.E. Rodrigues, Adsorption of carbon dioxide onto hydrotalcite-like compounds (HTlcs) at high temperatures, Ind. Eng. Chem. Res. 40 (2001) 204–209.

[10] M.K. Ram Reddy, Z.P. Xu, G.Q. Lu, J.C. Diniz Da Costa, Influence of water on high-temperature CO2 capture using layered double hydroxide derivatives, Ind. Eng. Chem. Res. 47 (2008) 2630–2635.

[11] Y. Ding, E. Alpay, Equilibria and kinetics of CO2 adsorption on hydrotalcite adsorbent, Chem. Eng. Sci. 55 (2000) 3461–3474.

[12] J.R. Hufton, S. Mayorga, S. Sircar, Sorption-enhanced reaction process for hydrogen production, AIChE J. 45 (1999) 248–256.

[13] H.T.J. Reijers, S.E.A. Valster-Schiermeier, P.D. Cobden, R.W. Van Den Brink, Hydrotalcite as CO2 sorbent for sorption-enhanced steam reforming of methane, Ind. Eng. Chem. Res. 45 (2006) 2522–2530.

[14] Y.J. Wu, P. Li, J.G. Yu, A.F. Cunha, A.E. Rodrigues, K-Promoted hydrotalcites for CO2 capture in sorption enhanced reactions, Chem. Eng. Technol. 36 (2013) 567–574.

[15] M.K.R. Reddy, Z.P. Xu, G.Q. Lu, J.C. Diniz da Costa, Effect of SOx adsorption on layered double hydroxides for CO2 capture, Ind. Eng. Chem. Res. 47 (2008) 7357–7360.

[16] M.G. Beaver, High temperature CO2 chemisorbents: applications, characterization, and study of the chemical nature of chemisorbent surfaces, Lehigh University, 2010.

[17] E. Van Dijk, S. Walspurger, P. Cobden, R. Van Den Brink, Testing of hydrotalcite based sorbents for CO2 and H2S capture for use in sorption enhanced water gas shift, Int. J. Greenhouse Gas Control 5 (2011) 505–511.

[18] J.R. Hufton, S. Mayorga, T. Gaffney, S. Nataraj, M. Rao, S. Sircar, Sorption enhanced reaction process for production of hydrogen, in: Proceedings of the 1998 U.S. DOE Hydrogen Program Review, 1998, pp. 693–705.

[19] V. Rives, Comment on ‘‘direct observation of a metastable solid phase of Mg/Al/CO3-layered double hydroxide by means of high-temperature in situ powder XRD and DTA/TG’’, Inorg. Chem. 38 (1999) 406–407.

[20] V. Rives, Characterisation of layered double hydroxides and their decomposition products, Mater. Chem. Phys. 75 (2002) 19–25.

[21] M.H. Halabi, M.H.J.M. De Croon, J. Van Der Schaaf, P.D. Cobden, J.C. Schouten, High capacity potassium-promoted hydrotalcite for CO2 capture in H2 production, Int. J. Hydrogen Energy 37 (2012) 4516–4525.

[22] M.K. Ram Reddy, Z.P. Xu, G.Q. Lu, J.C.D. Da Costa, Layered double hydroxides for CO2 capture: structure evolution and regeneration, Ind. Eng. Chem. Res. 45 (2006) 7504–7509.

[23] J. Rocha, M. Del Arco, V. Rives, M.A. Ulibarri, Reconstruction of layered double hydroxides from calcined precursors: a powder XRD and 27Al MAS NMR study, J. Mater. Chem. 9 (1999) 2499–2503.

[24] K. Chibwe, W. Jones, Intercalation of organic and inorganic anions into layered double hydroxides, J. Chem. Soc., Chem. Commun. (1989) 926–927.

[25] T. Kwon, T.J. Pinnavaia, Pillaring of a layered double hydroxide by polyoxometalates with Keggin-ion structures, Chem. Mater. 1 (1989) 381–383.

[26] M. Bellotto, B. Rebours, O. Clause, J. Lynch, D. Bazin, E. Elkaïm, Hydrotalcite decomposition mechanism: a clue to the structure and reactivity of spinel-like mixed oxides, J. Phys. Chem. 100 (1996) 8535–8542.

[27] E.C. Kruissink, L.L. van Reijen, J.R.H. Ross, Coprecipitated nickel–alumina catalysts for methanation at high temperature. Part 1. Chemical composition and structure of the precipitates, J. Chem. Soc., Faraday Trans. 1: Phys. Chem. Condens. Phases 77 (1981) 649–663.

[28] K.B. Lee, A. Verdooren, H.S. Caram, S. Sircar, Chemisorption of carbon dioxide on potassium-carbonate–promoted hydrotalcite, J. Colloid Interface Sci. 308 (2007) 30–39.

[29] Z. Yong, V. Mata, A.E. Rodrigues, Adsorption of carbon dioxide at high temperature – a review, Sep. Purif. Technol. 26 (2002) 195–205.

[30] N.D. Hutson, B.C. Attwood, High temperature adsorption of CO2 on various hydrotalcite-like compounds, Adsorption 14 (2008) 781–789.

[31] J.L. Soares, G.L. Casarin, H.J. José, R.D.F.P.M. Moreira, A.E. Rodrigues, Experimental and theoretical analysis for the CO2 adsorption on hydrotalcite, Adsorption 11 (2005) 237–241.

[32] D.D. Do, Adsorption Analysis: Equilibria and Kinetics, Imperial College Press, London, 1998.

[33] H. Du, A.D. Ebner, J.A. Ritter, Pressure dependence of the nonequilibrium kinetic model that describes the adsorption and desorption behavior of CO2 in K- promoted hydrotalcite like compound, Ind. Eng. Chem. Res. 50 (2011) 412–418.

[34] H. Du, C.T. Williams, A.D. Ebner, J.A. Ritter, In situ FTIR spectroscopic analysis of carbonate transformations during adsorption and desorption of CO2 in K-promoted HTlc, Chem. Mater. 22 (2010) 3519–3526.

[35] J. Crank, The Mathematics of Diffusion, second ed., Oxford University Press, London, 1975.